Journal Pre-proof

A dual-responsive biosensor for blood lead detection

Huan Chen, Shuibin Shao, Yueqi Yu, Yangyang Huang, Xiaotan Zhu, Shiyan Zhang, Jin Fan, Guo Yong Yin, Bo Chi, Mimi Wan, Chun Mao

PII: S0003-2670(19)31149-3

DOI: https://doi.org/10.1016/j.aca.2019.09.062

Reference: ACA 237115

To appear in: *Analytica Chimica Acta*

Received Date: 22 August 2019

Accepted Date: 23 September 2019

Please cite this article as: H. Chen, S. Shao, Y. Yu, Y. Huang, X. Zhu, S. Zhang, J. Fan, G.Y. Yin, B. Chi, M. Wan, C. Mao, A dual-responsive biosensor for blood lead detection, *Analytica Chimica Acta*, https://doi.org/10.1016/j.aca.2019.09.062.

A dual-responsive biosensor for blood lead detection

Huan Chen[a], Shuibin Shao[a], Yueqi Yu[a], Yangyang Huang[a], Xiaotan Zhu[a], Shiyan Zhang[a], Jin Fan[b], Guo Yong Yin[b], Bo Chi[c], Mimi Wan[a]*, Chun Mao[a]*

[a]*National and Local Joint Engineering Research Center of Biomedical Functional Materials, School of Chemistry and Materials Science, Nanjing Normal University, Nanjing, 210023, China.*

[b]*Department of Orthopaedics, The First Affiliated Hospital of Nanjing Medical University, Nanjing, 211166, China.*

[c]*State Key Laboratory of Materials-Oriented Chemical Engineering, College of Food Science and Light Industry, Nanjing Tech University, Nanjing 211816, China.*

* Corresponding author at: Nanjing Normal University, National and Local Joint Engineering Research Center of Biomedical Functional Materials, No. 1 Wenyuan Road, Nanjing, 210023, China.

Email: M. M. Wan (Email: wanmimi@njnu.edu.cn), C. M. (Email: maochun@njnu.edu.cn).

ABSTRACT

Simple and accurate detection of trace heavy metals in blood is very important. A novel dual-responsive electrochemical/fluorescent biosensor based on magnetic hyperbranched polyamide with heparin modification (MHPAM-H) for blood lead detection has been successfully developed. Upon conjugated with blood lead ions, dual-biosensor could not only display electrochemical signal but also fluorescence signal owing to the enriched amino groups, cavity structure, and good fluorescence properties of HPAM. Blood biocompatibility, construction of the dual-responsive biosensor, electrochemical/ fluorescent detection of lead ions in water phase and blood condition, selectivity and stability of the dual-responsive biosensor were investigated in detail. The proposed dual-responsive biosensor displays good linear relationship (1.5 pM- 4.8×10^3 pM for electrochemical detection and 0.5 pM-4.8×10^3 pM for fluorescent detection) with low detection limit (4.4 pM for electrochemical detection and 1.0 pM for fluorescent detection) for blood lead, providing potential application for blood lead detection in the future.

Keywords: Dual-responsive biosensor, Electrochemical/ fluorescent detection, Blood lead ions, Blood compatibility

1. Introduction

Lead (Pb^{2+}) is one of the most toxic metal contaminants that can enter the bloodstream through critical organs and systems such as skin, digestive system and respiratory organs [1-5]. There are several widely used analytical methods for detecting lead levels, such as atomic absorption spectroscopy (AAS), inductively coupled plasma atomic emission spectroscopy (ICP-AES), and so on, which often require complex instruments and tedious sample pretreatment procedures [6-11]. Current researchers are making unremitting efforts to develop rapid, reliable and economical techniques for the determination of blood lead. As blood is a system with complex physiological environment, the detection of blood lead usually requires complex pretreatment of samples (such as digestion of blood samples with strong acid and high temperature) [12, 13]. The operation process is cumbersome and the use of a large amount of acid causes environmental pollution. Hence, it is of great significance to develop a new, convenience and accurate technique for detecting blood lead rapidly and directly.

Plenty of lead biosensors (water phase) have been developed in recent decades, which are focused on electrochemical and fluorescent biosensors [14-18]. However, these biosensors cannot directly detect lead in blood. Generally, when traditional biosensors contact with a complex blood environment directly, the adhesion of proteins and red blood cells may cause contamination of the biosensors, thereby affecting the detection accuracy [19]. Meantime, owing to the fact that each method has its own advantages and limitations, a synergistic combination of two or more detection methods may result in much more convincing results and the detection results can be normalized and obtained with dual-responsive biosensors [20].

Herein, a dual-responsive biosensor denoted as magnetic hyperbranched polyamide with

heparin modification (MHPAM-H) which can be used for electrochemical/fluorescence detection of blood lead was proposed in this work (Scheme 1). In this system, the presence of magnetic Fe_3O_4 can realize the rapid immobilization of the biosensor on the magnetic electrodes. While hyperbranched polyamides (HPAM) with enriched amino groups, cavity structure, and good fluorescence properties have the ability to rapidly accumulate blood lead by forming coordinate bond with lead ions (within 5 min), providing the possibility to quickly and stably detect blood lead [21]. The electrochemical detection principle is based on the fact that the enriched lead ions will be precipitated on the electrode surface to produce current. As a fluorescent substance, HPAM has the advantages of continuous/wide absorption band, good water solubility and good biocompatibility compared with traditional organic dyes, and is potential to be used for the detection of biomedical fields [22, 23]. Lead ions captured by HPAM can form coordination bonds with amino groups in HPAM, which restricts the geometric movement of fluorescence centers to a certain extent, thus increasing the fluorescence intensity [24]. The modification of heparin provides biofouling resistance of the biosensor in the blood environment [25]. Compared with the traditional lead biosensor in aqueous phase, the dual-responsive biosensor for blood provided by this work can provide better repeatability, high sensitivity and good stability. More importantly, this method can be used to detect the concentration of blood lead directly without using tedious and complicated blood digestion steps and large instruments and the dual-responsive methods can be cross-validated to improve the reliability of the test data.

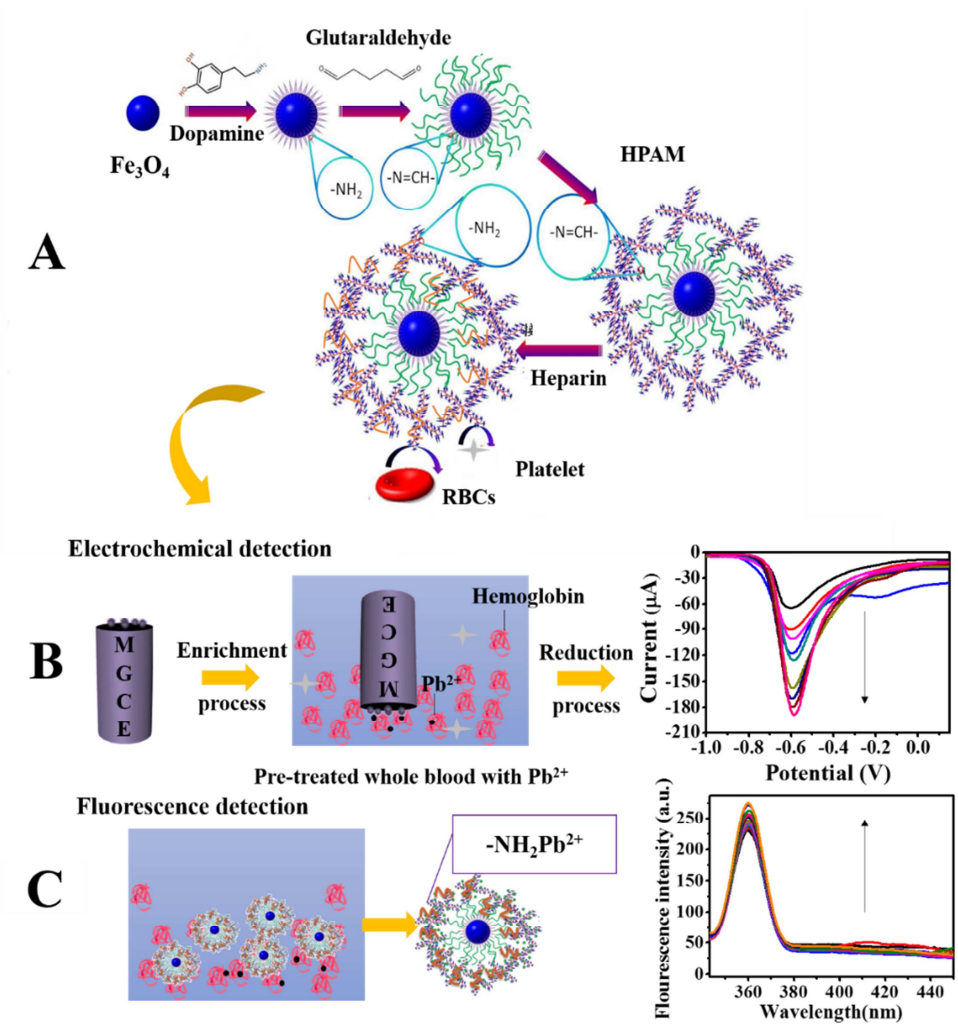

Scheme 1. (A) Schematic illustration of the synthesis of MHPAM-H NPs, and their applications in (B) the electrochemical detection and (C) the fluorescence detection for blood lead.

2. Experimental

2.1 Materials

Ferrous sulfate ($FeSO_4$•$7H_2O$) was obtained from Xilong chemical plant in Shantou of Guangdong (China). Polyethylene glycol (PEG)-20000 was bought from Aladdin chemical reagent Co. Ltd. in Shanghai (China). Hyperbranched polyamide (HPAM) was bought from Wuhan Hyperbranched polymers science and technology Co. Ltd. (China). Ammonium hydroxide, trimethylolamine (Tris) were purchased from Sinopharm chemical reagent Co. Ltd. in Shanghai

(China). Dopamine was bought from Alfa Aesar. lead ion concentration standard liquid was bought from General Research Institute for Nonferrous Metals (China). Dopamine hydrochloride (DA) and porcine heparin (MWCO 8000-12000) were purchased from Sigma-Aldrich Co. Ltd. (USA). Glutaraldehyde 25% (GA), monopotassium-phosphate (KH_2PO_4), disodium-hydrogen phosphate (Na_2HPO_4), potassium chloride (KCl) and sodium chloride (NaCl) were purchased from Sinopharm Chemical Reagent Co. Ltd (China) and used as received.

2.2 Synthesis of the MHPAM-H nanoparticles

2.2.1 Synthesis of Fe_3O_4 NPs

2.5 g of $FeSO_4 \cdot 7H_2O$ was dissolved in 30 mL of deionized water (DW) by ultrasonic and transferred to a round-bottom flask. After adding 10 mL of DW containing 0.5 g polyethylene glycol (PEG)-2000 to the preceding solution of $FeSO_4$, the reaction was kept at 30℃ with vigorous stirring and inert atmosphere. Next, 30 mL of ammonium hydroxide was added to the reaction and continued stirring for 10 min. 0.27 mL of hydrogen peroxide (30%) was added to the reaction subsequently for another 20 min of fierce stirring, and the solution was transferred to a reaction kettle at 160℃ for 5 h. The result precipitate was washed with DW and ethanol for several times, and dried under vacuum at 60℃.

2.2.2 Synthesis of MHPAM NPs

50 mg of Fe_3O_4 NPs were dispersed into 10 mL of Tris-HCl buffered saline (50 nM, pH=8.5) by ultrasonic, while 50 mg of dopamine was dissolved into 10 mL of Tris-HCl buffered saline (50 nM, pH=8.5) under dark condition. The two kinds of prepared solution were kept stirring to mix completely under dark condition for 2 h. Then the product was collected with magnets and washed with DW. After the material was re-dispersed into 10 mL of DW, 50 mL of glutaraldehyde solution

(6%) was added to the suspension while stirring for 12 h. The result precipitate was collected, washed with DW and added into 100 mL of hyperbranched polyamide solution (0.4 mg mL^{-1}) while stirring for 12 h. The final product was also collect with magnets, washed with DW and dried under reduced pressure.

2.2.3 Preparation of MHPAM-H with anticoagulation property

The MHPAM-H which possessed the property of anticoagulation was acquired by dispersing 10 mg of HPAM into heparin solution (4 mg mL^{-1}) equably for 12 h. Finally, the products were washed three times with DW, collected by centrifugation and dried for use.

2.3 Characterization of the MHPAM NPs

The morphology of Fe_3O_4 and MHPAM nanoparticles was observed by transmission electron microscopy (TEM) with an H-7650 interface high-resolution transmission electron micro (HITACHI, Japan). The structures were determined by Fourier transform infrared (FT-IR) spectra using a Cary 5000 Fourier transform infrared spectrophotometer (VARIAN, USA). The particle size and ζ-potential of the samples were also measured by Zetasizer Nano Z (Malvern, USA).

2.4 Biocompatibility evaluation

2.4.1 In vivo coagulation time analysis

The assays of coagulation of the MHPAM NPs and MHPAM-H NPs were inspected via activated partial thromboplastin time (APTT), prothrombin time (PT) and thrombin time (TT) [26]. The fresh blood was centrifuged at 4℃ to obtain the plasma containing few blood platelet. The Fe_3O_4 NPs, MHPAM NPs and MHPAM-H NPs were prepared into suspension with phosphate-buffered saline (PBS, pH= 7), and incubated with the treated plasma for 30 min. All the tests were conducted according to the manual of the kit. PBS was determined as the control and all

the tests were performed thrice.

2.4.2 Hemolysis assay

The Fe_3O_4 NPs, MHPAM NPs, and MHPAM-H NPs were dispersed into PBS and incubated for 24 h, after which the materials were collected and the liquid was discarded. Subsequent steps are as follows:

(1) The preparation of RBCs suspension: Fresh blood was centrifuged (1.5×10^3 rpm, 10 min) to achieve RBCs, which were washed 2 to 3 times subsequently with PBS until the supernatant was clear. Then the RBCs were diluted into suspension (2%).

(2) The treated materials were incubated with the suspension of RBCs for 1 h, and the supernatant was separated by centrifugation (1.5×10^3 rpm, 10 min), the UV absorption of which was detected at 545 nm by the UV-visible spectrophotometer. PBS acted as the negative control and DW was the positive control. All the tests were performed thrice. The formula of percent hemolysis is: Hemolysis (%) = $(OD_t-OD_{nc})/(OD_{pc}-OD_{nc})\times100\%$. OD_t referred to the absorption value of the samples, OD_{nc} represented the absorption value of the negative control and OD_{pc} was the absorption value of the positive control.

2.4.3 Whole blood adhesion test

The ITO (Indium Tin Oxides) glass electrode was used to replace magnetic glassy carbon electrode (MGCE) in whole blood adhesion test [27]. Polypyrrole (PPy)@electrode, MHPAM@PPy@electrode and MHPAM-H@PPy@electrode were laid out at the bottom of a 24-well culture plate. Then 1 mL of PBS was added into each well and balanced for 24 h. After removing the liquid, each well was added with 1 mL of whole blood and the samples were incubated with the blood at 37℃ for 30 min. PBS was used to wash the samples for 3 times after

the whole blood was separated, and glutaraldehyde (2.5%) was added into the wells to fix the samples for 30 min. Then ethanol with different concentrations (50, 60, 70, 80, 90, 95, 100%) were utilized to exsiccate the samples for 30 min. SEM was used to observe the morphologies of the samples.

2.5 Characterization of electrochemical and fluorescent properties of MHPAM-H

MHPAM-H aqueous solution was dispersed by ultrasound for 15 minutes. Then, a certain amount of homogeneous dispersion material was dripped onto the surface of the magnetic electrode which plated with polypyrrole (MHPAM-H@PPy@MGCE) and dried naturally at room temperature. By comparison, bare magnetic electrode (MGCE), MHPAM-H modified MGCE (MHPAM-H @MGCE), polypyrrole electroplated magnetic electrode (PPy@MGCE) were prepared with a similar process [28]. Cyclic voltammograms (CVs) were performed in $K_3[Fe(CN)_6]$ (5.0 mM) and KCl (0.1 M) from -0.2 V to 0.7 V, with a scan rate of 100 mV s^{-1}. The electrochemical impedance spectroscopy (EIS) tests were carried out to monitor changes of the electrode surface with the frequency ranging from 1 Hz to 100 kHz, and performed in PBS (0.1 M) comprising $[Fe(CN)_6/Fe(CN)_6]^{3-/4-}$ (10 mM) and KCl (0.1 M). All electrochemical measurements were performed by electrochemical workstation (CHI 760D, Chenhua, Shanghai, China). The fluorescence spectra of samples were collected by fluorescence spectrophotometer (F-4600, Hitachi Corporation of Japan) with excitation wavelength at 320 nm.

2.6 Optimization of the biosensor

2.6.1 Optimization of the electrochemical detection conditions of dual-responsive biosensor

The electrochemical property of the biosensor under a series of different conditions such as buffer solution (PBS, NH_4Cl-$NH_3 \cdot H_2O$, NaAc-HAc, Tris-HCl), amounts of material (4.0 μL, 8.0

μL, 16.0 μL, 20.0 μL), and pH values (4, 5, 6, 7, 8, 9) for lead ions detection were investigated by differential pulse voltammetry (DPV) method.

2.6.2 Optimization of the fluorescence detection conditions of dual-responsive biosensor

The fluorescent property of the biosensor were measured under a series different conditions such as concentrations of material (20, 30, 40, 50 μg mL^{-1}), excitation wavelengths (320, 340, 360, 380, 400 nm), and different pH values (4, 5, 6, 7, 8, 9) when detection of lead ions (4800 pM).

2.7 Measurements by dual-responsive biosensors

2.7.1 Electrochemical detection of lead in water phase

The connections between current signals and different concentrations of which were obtained by DPV, with pulse amplitude of 0.05 V and pulse frequency of 0.05 V and the voltage ranges from -1.0 V to 0.2 V, scanning for 50 seconds. It were recorded under the best experimental condition (PBS, pH=7, 8.0 μL of the material). All the tests related to electrochemistry were conducted in a three-electrode system: The modified magnetic glassy carbon electrode was used as the working electrode, the saturated calomel electrode (SCE) and the Pt wire was acted as the reference electrode and the counter electrode.

2.7.2 Electrochemical detection of lead in whole blood

Rabbit blood containing different concentration of lead ion was prepared with PBS buffer solution (pH=7). Then the functionalized working electrode was immersed into the solutions of $Pb^{2+}$of disparate concentrations and tested after 5 min. The detection method is the same as that in aqueous phase.

2.7.3 Fluorescent detection of in water phase

MHPAM (20.0 μL, 1 mg mL^{-1}) was added to the aqueous solution containing different

concentration of lead ions, and mixed in a silent mixer for 5 minutes. And then, the fluorescence spectra of samples were detected by fluorescence spectrophotometer (F-4600, Hitachi Corporation of Japan), excitation wavelength at 320 nm, Scan speed is 1200 nm/min.

2.7.4 Fluorescent detection of lead in whole blood

The standard solution of lead was added to the rabbit blood and diluted 10000 times with PBS (0.1 M) and KCl (0.1 M, pH=7) to prepare rabbit blood solution with different concentrations of lead ion. The solution for detection in whole blood was prepared by adding 20.0 μL of MHPAM-H (1 mg mL^{-1}) into the solution containing different concentrations of lead ions respectively. The solution was mixed by mixer and stabilized for 5 min before the fluorescent detection. And then, the fluorescence spectra of samples were detected by fluorescence spectrophotometer (F-4600, Hitachi Corporation of Japan), excitation wavelength at 320 nm, Scan speed is 1200 nm/min.

2.8 Interference and stability study

Individual ions (Pb^{2+}, Mn^{2+}, Zn^{2+}, Cu^{2+}, Fe^{3+}) and mixed ions (Pb^{2+}+Mn^{2+}， Pb^{2+}+ Zn^{2+}, Pb^{2+}+ Cu^{2+}, Pb^{2+}+ Fe^{3+}) in water and in whole blood were detected by fluorescence biosensor. The mixed heavy metal ions (Pb^{2+}+Mn^{2+}， Pb^{2+}+ Zn^{2+}, Pb^{2+}+ Cu^{2+}, Pb^{2+}+ Fe^{3+}) in aqueous solution and whole blood were detected by electrochemical biosensor. Stability was a significant parameter to evaluate biosensors and the changes of current signals were inspected by scanning the CV curve for 200 times.

3. Results and discussion

3.1 Characterizations of MHPAM NPs

The morphologies of MHPAM and Fe_3O_4 were characterized by TEM technique and the statistical analyses for TEM images with 25 particles were summarized, which displays that the

size of Fe_3O_4 is around 32.3±5.6 nm, and after the modification of HPAM, the size of MHPAM is 36.6±6.7 nm with similar morphology (Fig. 1A, 1B and Fig. S1). SEM images and energy dispersive spectroscopy (EDS) also verified the existence of C, N, Fe elements, indicating successful modification of HPAM (Fig. 1C and 1D).

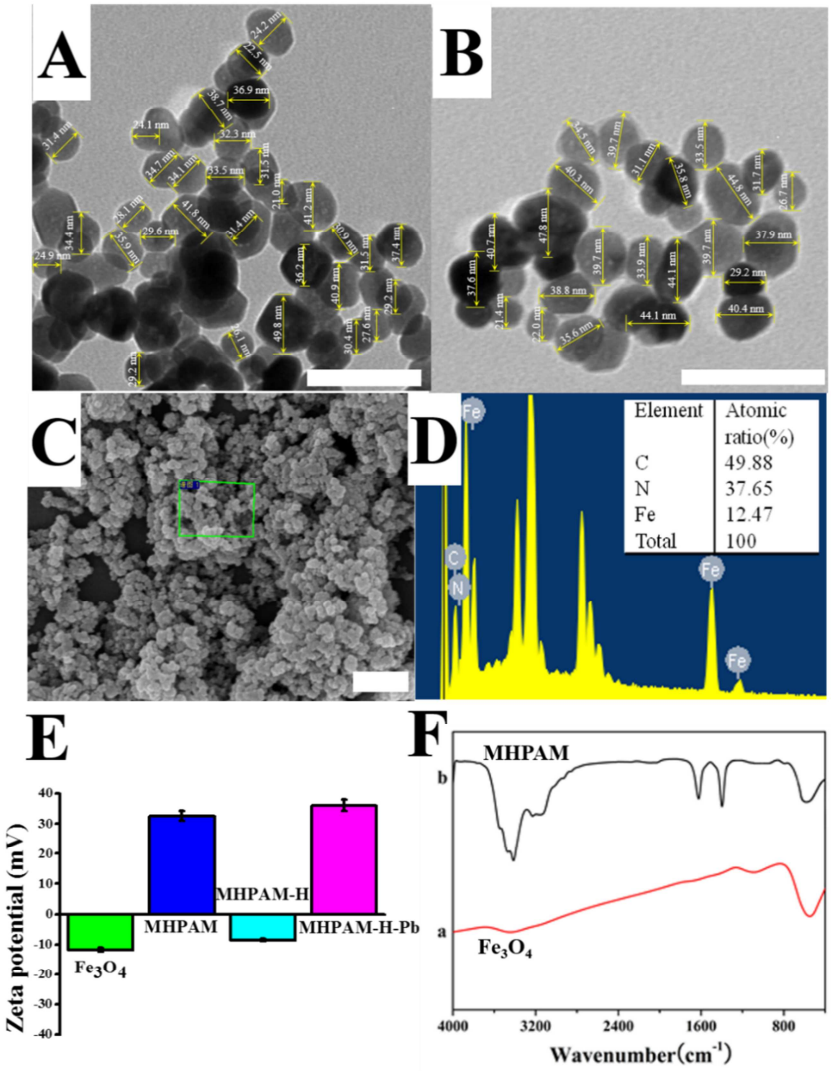

Fig. 1. TEM images of (A) Fe_3O_4 and (B) MHPAM NPs (Scale bar: 100 nm); (C) SEM image and (D) SEM-EDS spectrum of MHPAM NPs (Scale bar: 1 μm); (E) Zeta potentials of the samples; (F) FT-IR spectra of (a) Fe_3O_4 and (b) MHPAM, respectively.

Zeta potential changes from around -11.7 mV (Fe_3O_4 NPs) to around +32.2 mV for MHPAM

(Fig. 1E), which is likely resulted from the charge screening effect caused by the exposure of large amounts of amino groups on the surface of HPAM, indicating the successful modification of HPAM on the surface of Fe_3O_4 NPs coating process. With the negatively charged heparin grafted onto MHPAM (MHPAM-H), MHPAM-H shows negative charge (-9.8 mV), confirming the successful loading of heparin. In addition, when MHPAM-H NPs adsorbs lead ions, its zeta potential changes to +33 mV, indicating that the MHPAM-H can effectively capture lead ions.

The functionalization of magnetic Fe_3O_4 NPs with HPAM was further characterized by the FTIR spectra (Fig 1F). The characteristic absorption peak of Fe-O appears at 560 cm^{-1} [29]. The successful modification of HPAM was confirmed by the existence of C=O stretching vibration peak at 1630 cm^{-1} and amino functional group peak at 1400-1600 cm^{-1} [30].

In addition, the morphologies of the electrode with the addition of MHPAM-H were also characterized by SEM images. As shown in Fig. S2, the surface of bare electrode is smooth, and distinct striations can be observed after polypyrrole was plated on the surface of the electrode. Obvious granular substances can be observed on the electrode after MHPAM NPs was added, implying the successful construction of the electrode.

3.2 Biocompatibility analysis

3.2.1 In vivo coagulation time analysis

Blood compatibility is the basic requirement of blood contacting materials. APTT, PT and TT are widely used to detect the abnormality of blood plasma [31]. As shown in Fig. 2A, compared with the negative control (12.0 s), the coagulation time of MHPAM is slightly shorter (10.2 s). The values of APTT, PT and TT are 24.8, 7.3 and 20.2 s after injection of MHPAM-H NPs, indicating good anticoagulant property of MHPAM-H. This could be due to heparin with good anticoagulant

effect was successfully loaded from HPAM with enriched amino groups and cavity structure [32, 33].

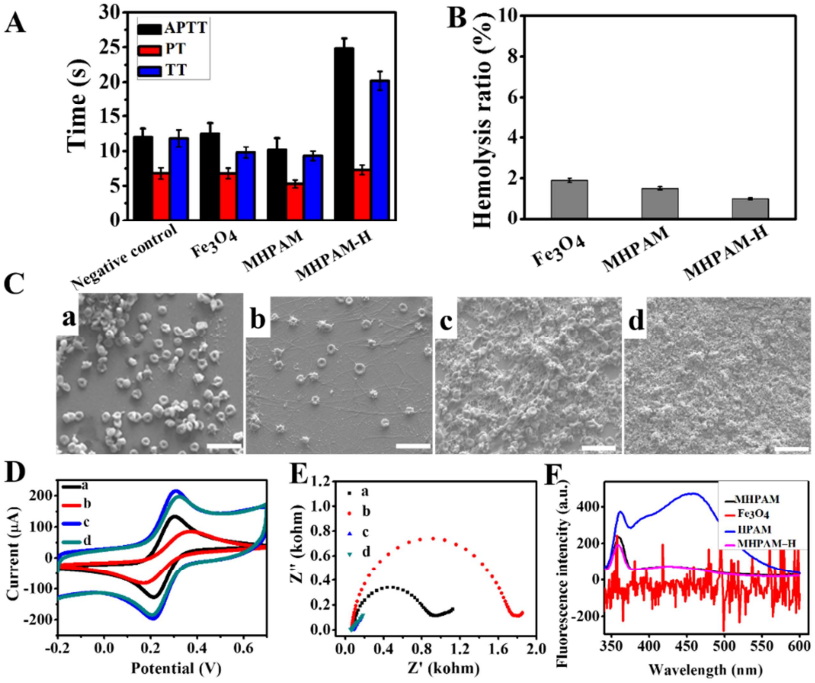

Fig. 2. (A) *In vitro* coagulation time of negative control, Fe_3O_4, MHPAM and MHPAM-H; (B) Hemolysis test results of Fe_3O_4, MHPAM, and MHPAM-H; (C) SEM images of whole blood adhesion for (a) bare electrode, (b) PPy@bare electrode, (c) MHPAM@PPy@bare electrode and (d) MHPAM-H@PPy@bare electrode (Scale bar: 20 μm); (D) CVs and (E) EIS spectra of (a) MGCE, (b) MHPAM-H@MGCE, (c) PPy@MGCE, (d) MHPAM-H@PPy@MGCE in pH= 7 PBS containing 0.1 M KCl and 5 mM $Fe(CN)_6^{3-}/Fe(CN)_6^{4-}$ (F) Fluorescence spectra of Fe_3O_4, HPAM, MHPAM, and MHPAM-H.

3.2.2 Hemolysis assay

The hemolysis rate test was further used to verify the blood compatibility of the materials [34]. In our research, the hemolysis rates of samples are all less than 5% and it can be reduced more effectively by anticoagulant treatment with heparin (1.3%), implying good blood compatibility of

MHPAM-H (Fig. 2B). This may due to the loading of heparin the positive charge on the surface of the polymer was partially shielded and the interaction between polyamide and erythrocyte surface was reduced [35].

3.2.3 Whole blood adhesion test

Anti-biofouling property of the modified electrode surface was evaluated by whole blood adhesion tests [36]. The SEM results indicate that a large number of RBCs and platelets are adhered to the surface of the bare electrode, PPy@electrode, MHPAM@PPy@electrode. On the contrary, the surface of the electrode modified with MHPAM-H NPs is much cleaner (Fig. 2C), indicating good anti-fouling property of MHPAM-H NPs and providing an opportunity for MHPAM-H NPs to detect analytes in whole blood environments directly.

3.3 Electrochemical and fluorescence properties characterization of the MHPAM-H NPs

3.3.1 Electrochemical behavior of MHPAM-H NPs

In order to investigate the assembly process of biosensors, the cyclic voltammograms (CV) was presented in Fig. 2D for different samples during the construction process of the electrode [37]. Compared with bare electrode (curve a), the peak current of MHPAM-H@MGCE (curve b) decreases obviously. While the peak current of PPy@MGCE (curve c) increases significantly, which proves that the introduction of conductive polymer PPy can enhance the conductivity of the biosensor. The peak current value of MHPAM-H@PPy@MGCE (curve d) decreases a little, which is due to the barrier formed by the introduction of MHPAM-H, thus decreases the access of $K_3[Fe(CN)_6]/K_4[Fe(CN)_6]$ from the bulk solution to the electrode interface.

Successful construction of the electrode can also be verified by EIS results, which display the changes of the interface between working electrodes and electrolytes during the stepwise

construction of the biosensors [38]. A semicircle which from Nyquist plot meaning that the charge transfer resistance cause by redox reaction on the surface of the electrode. The larger diameter of the semicircle, the greater the resistance of the electrode [39]. Fig. 2E displays the Nyquist plots for different modification stages. The impedance spectrum of the bare electrode was shown in curve a. Compared with bare electrodes, the diameter of the semicircle increases when the surface of the electrode was modified by MHPAM-H with poor electrical properties (curve b). Owing to the great conductivity of PPy, the resistance of modified PPy electrode reduced a lot, and the diameter of the semicircle in the high frequency region decreases a lot (curve c). Similarly, when the electrode surface is modified by MHPAM-H and PPy, its resistance decreases (curve d). Because the electrochemical reaction is heterogeneous [40], the size and state of the interface have a great influence on its electrochemical reaction. Here, the active surface area of the electrode was calculated according to Randles-Sevcik formula by measuring the current value at scan rates from 10 mV s^{-1} to 200 mV s^{-1} and the linear relationship between peak current and the square root of scan rate. The formula is as follows: $I_p=(2.69*10^5)n^{3/2}ACD^{1/2}\nu^{1/2}$ where I_p represents the peak current (A), n stands for the number of electrons transferred in the redox process (n = 1 in this work), A is the effective surface area (cm^2), C is K^+ concentration in the electrode (mol cm^{-3}), D is the diffusion coefficient of K^+ (cm^2 s^{-1}), and ν is the scan rate ($V\cdot s^{-1}$) [41]. As shown in Fig. S3, the electrochemical active surface areas of the bare electrode, PPy@MGCE, MHPAM-H@MGCE and MHPAM-H@PPy@MGCE were calculated for 0.1 cm^{-2}, 1.5×10^{-1} cm^{-2}, $4.9\times10^{-2}cm^{-2}$ and 1.2×10^{-1} cm^{-2}, respectively. The results show that the design of conductive polymer polypyrrole can increase the active surface area of the GCE, enhancing the conductivity of the electrode and providing conditions for improving the sensitivity of the biosensor [42].

3.3.2 The fluorescence properties of the MHPAM-H NPs

As shown in Fig. 2F pure Fe_3O_4 displays no fluorescence property under the excitation wavelength of 320 nm. There are two main peaks located at around 360 and 450 nm for the fluorescence spectrum of HPAM. The fluorescence spectrum of MHPAM is similar to that of HPAM with the weakened peak intensity, verifying fluorescence property of MHPAM-H. After being immobilized on magnetic particles, the peak intensity decreased a lot, which may be attributed to the fact that the relative extinction coefficient of metal oxide particles was improved greatly by combining with polymer may cause fluorescence quenching of HPAM to some extent [43]. Meantime, the intraparticle energy transfer between the HPAM and magnetic nanoparticles may also decrease the fluorescence intensity. The relative sharp peak located at 360 nm was chosen as the main peak to study the response of fluorescent MHPAM to blood lead.

3.4 Optimization of the dual-responsive biosensor

3.4.1 Optimization of the electrochemical detection conditions of biosensor

The electrochemical detection results of biosensors are commonly affected by many factors. DPV method is used to measure the effect of different buffer solution, different amounts of materials and pH values of the PBS buffer solution to determine the optimized condition for electrochemical detection. Fig. 3A (a) shows that in different buffer solution systems (PBS, NH_4Cl-$NH_3.H_2O$, NaAc-HAc, Tris-HCl) with pH value of 7 and the current value under PBS buffer solution is the largest. The effect of different buffer solutions on current signals may be due to the different charge transfer resistance (R_{ct}) of buffer solutions [44]. The electrochemical impedance spectroscopy (EIS) of different buffer solutions were detected, which indicated that PBS buffer solution as electrolyte displayed the smallest R_{ct} in several buffer solutions, so its

current signal was the strongest in this system (Fig. S4). The amount of biosensor also has a direct impact on the current signal of the electrode, too small amount is not conducive for the enrichment of analytes, while too much may hinder the transmission of electrons. Fig. 3A (b) shows that the current reaches the maximum value when the added material is 8.0 μL. When the electrolyte was PBS buffer solution, the different pH values of the electrolyte will cause the change of current signal, which may be due to the difference of the binding state of MHPAM with lead ion and the state of lead ion itself (Fig. 3A, c). At low pH values (4-5), attributed by a large number of amino groups in MHPAM are protonated, which made it difficult for MHPAM to bind lead ions because of electrostatic repulsive forces for active sites [45]. Therefore, the electrochemical signal becomes weak. With the increase of pH value (6-7), the amino group of MHPAM can bind to lead ions effectively, thus the electrochemical signal increases. But with further increase of pH value (8-9), the response of dual-responsive biosensor will be reduced because of lead ions will be precipitated in the form of hydroxide when pH values rose above 7.0 [46]. In sum, the dual-responsive biosensor has the best signal response in the suitable pH range (≈7) because MHPAM has high adsorption efficiency for lead ions, which provides theoretical support for the detection of lead ion in blood as the pH value of human blood environment is close to 7. Therefore, the PBS buffer solution with pH value of 7 and material dosage of 8.0 μL are selected as the experimental conditions for electrochemical detection in the following measurement.

3.4.2 Optimization of the fluorescence detection conditions of biosensor

The effects of different concentrations of material (20, 30, 40, 50 μg mL^{-1}), different detection excitation wavelength (320, 340, 360, 380, 400 nm) and pH values (4, 5, 6, 7, 8, 9) for lead ions fluorescence detection were also investigated. As shown in Fig. 3B, the fluorescence intensity of

MHPAM-H decreases slightly with the increase of MHPAM-H concentration and there is a maximum emission peak while excitation wavelength at 320 nm. Moreover, the result of fluorescence signal response of MHPAM-H to lead ions under different pH show that it is consistent with the trend of electrochemical detection: the dual-responsive biosensor has the best signal response in the suitable pH range (≈7, Fig. S5). Therefore, the PBS buffer solution with pH value of 7 and material's concentration of 20 μg mL^{-1}, excitation wavelength at 320 nm are selected as the experimental conditions for fluorescence detection in the following measurement.

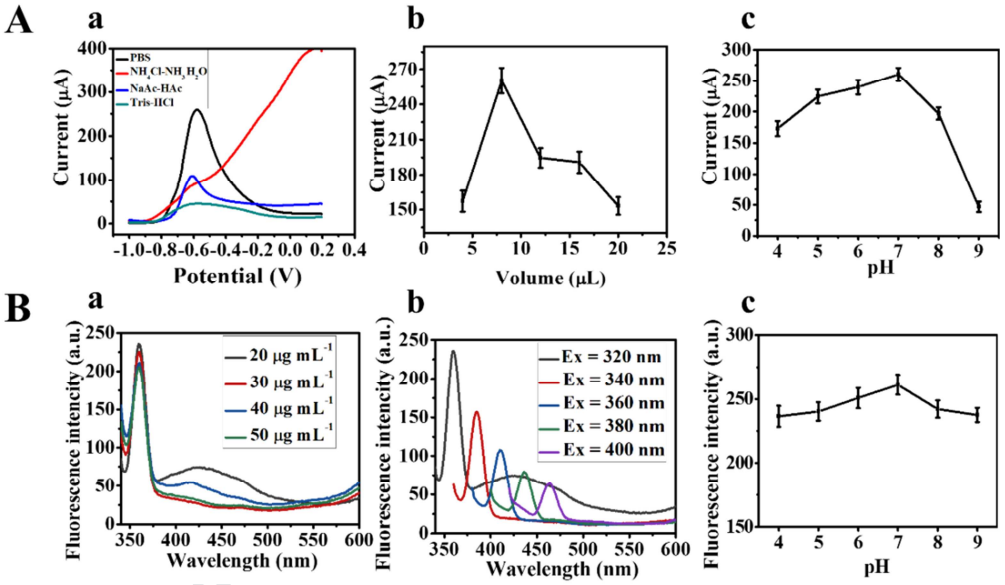

Fig. 3. (A) The optimization of electrochemical detection conditions: (a) different buffer solution, (b) different amount of materials and (c) different pH values for lead ions detection; (B) The optimization of fluorescence detection conditions: (a) different amounts of material, (b) different excitation wavelength and (c) different pH values for lead ions detection.

3.5 Analytical performance of the biosensor

3.5.1 Electrochemical detection of lead ions in water phase

Because MHPAM has the ability to rapidly and efficiently enrich lead ions [47], the

electrochemical detection principle is based on the rapid enrichment of lead ions by MHPAM (within 5 min), and the enriched lead ions will be precipitated on the electrode surface, generating a current. Therefore, the absolute value of the current increases with the lead ion concentration. DPV was used for discussion of the change of current signal here. Under the optimum detection conditions (PBS solution, pH=7, 8.0 μL of the material droplet dosage), the relationship between current signal and lead concentration was recorded. As show in Fig. 4A, the absolute value of the response current of the biosensor increases with the increasing concentrations of lead ions. The calibration plot shows a good linear relationship between the peak currents and the logarithm values of the lead concentrations in the range from 50 pM to 4.8×10^4 pM. The regression equation is y (I, μA) = -65.98 lg (c, pM) +63.32, (R^2=0.99) (Fig. 4B) indicating that the dual-responsive biosensors we prepared exhibits excellent electrochemical performance under water phase.

3.5.2 Electrochemical determination of lead ions in blood

In order to explore the electrochemical performance of the biosensor in the blood environment, the MHPAM-H@PPy@MGCE was exposed to whole blood containing different concentrations of lead. DPV signal was collected after the enrichment process of lead ions for 5 min. As expected, with the increase of lg (c, pM) from 0.2 to 3.7, which means lead concentration increases from 1.5 pM to 4.8×10^3 pM , the current response increases with blood lead concentration (Fig. 4C). Owing to the complex components of the blood, current response of the biosensor in blood condition is slightly lower than that in water phase. But the current peak appears in the same position, which shows that the dual-response sensor in the complex system of blood still has a good ability of detecting lead ions. Moreover, as displayed in Fig. 4D, a linear relationship between the amperometric response and the lead ion concentration was obtained. The regression equation is y(I,

μA)= -35.28lg(c, pM)+59.25 (R^2=0.99), and the limit of detection (LOD) and limit of quantification (LOQ) for lead ion were 4.4 pM and 14.7 pM (based on signal to noise ratio S/N = 3) that calculated with the equation: LOD = 3σ/k, LOQ =10 σ/k; where σ is the standard deviation of blank measurements, k is the slope of the calibration curve [48, 49], which is much lower than that of other lead sensors in water phase reported by other literatures (Table S1).

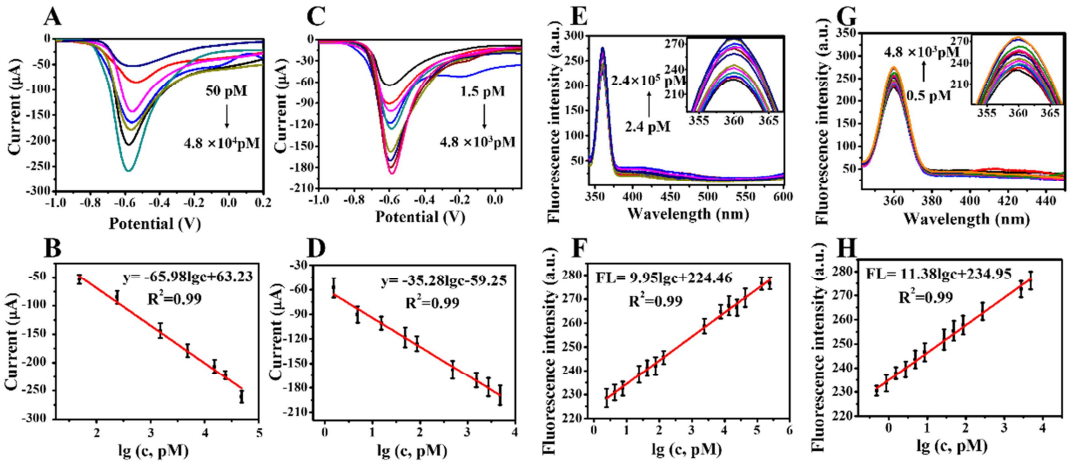

Fig. 4. (A) The DPV curve of different lead concentration (50 pM-4.8×10^4 pM) and (B) the calibration curve of the biosensor for different concentrations of lead under water solution; (C) The DPV curve of different lead concentration (1.5 pM-4.8×10^3 pM) and (D) the calibration curve of the biosensor for different concentrations of lead under the whole blood. (E) Fluorescence spectra of the interaction of MHPAM with different concentrations of (2.4 pM-2.4×10^5 pM) lead in aqueous phase; (F) Logarithmic relation of fluorescence intensity/lead Concentration; (G) Fluorescence spectra of the interaction between MHPAM and lead at different concentrations (0.5 pM-4.8×10^3 pM) in whole blood; (H) the relationship between logarithm of lead concentration and fluorescence intensity.

3.5.3 Fluorescence determination of lead ions in water

As shown in Fig. 4E and 4F, fluorescence intensity and lg(c, pM) shows a good linear curve (R^2

= 0.99) in the range of 2.4 pM-2.4×10^5 pM of lead ion concentration in aqueous phase. The fluorescence intensity of MHPAM-H increases with lead concentration, which may due to the following reasons: (1) Lead ions captured by HPAM can form coordination bonds with amino and carbonyl groups in HPAM, which restricts the geometric movement of fluorescence centers to a certain extent, thus increasing the fluorescence intensity [24]. (2) Lead ions are encapsulated by the cavity in HPAM, which promotes the formation of fluorescence center and enhances its fluorescence intensity.

3.5.4 Fluorescence determination of lead ions in blood

Meantime, in the blood environment, the fluorescence intensity and lg(c, pM) show a good fitting linear curve (R^2=0.99) in the range of lead ion concentration of 0.5 pM-4.8×10^3 pM (Fig.4G and 4H). The difference of linear range between water phase and blood may be related to the different states of lead ions in water phase and blood. In aqueous solution, lead ions are free and exist in the form of hydrated lead ions, so it is very difficult to capture them at very low lead ion concentration, which usually requires high-density adsorption sites [50]. In the blood environment, most of the lead ions are bound to hemoglobin in blood (one hemoglobin can bind at least four lead ions) [47], which is the enrichment of lead ions to a certain extent. To a certain extent, this enrichment of lead ion may amplify the detection signal of the sensor. That may be the reason that the lowest concentration of lead ions detected by electrochemical sensors or fluorescent sensors in blood is lower than that in water phase.

In particular, since the fluorescent HPAM used in the present work has a high density of active groups such as amino and carbonyl groups which can specifically bind with lead ions, the fluorescent sensor exhibits far lower LOD and LOQ for lead ion was as low as 1.0 pM and 3.3 pM

(Table S2). Table S1 and S2 summarizes the linear range, LOD and LOQ for the detection of lead ions by different lead ion sensors (electrochemical and fluorescent sensors) in aqueous condition. At present, there is no lead ion sensor that can be used for whole blood detection, and the active components of most fluorescent sensors are DNA or noble metal nanoclusters. Compared with most of the materials currently used for lead ion sensors in aqueous phase, most of them can only achieve one-response mode (electrochemical or fluorescent detection). The blood lead ion biosensor proposed in this work can not only rapidly enrich lead ions, but also have good fluorescence performance because of its unique hyperbranched structure, achieving two kinds of responsive modes for the detection of blood lead ions. The LOD and LOQ of the sensor we prepared in blood environment (electrochemical biosensor are 4.4 pM and 14.7 pM; fluorescent biosensor are 1.0 pM and 3.3 pM) lower than most of the detection limit of the biosensors proposed in other literatures, illustrating good ability for the dual-responsive biosensor proposed in this work to detect low-concentration lead ions.

3.6 Interference and stability study

Our speculations are as follows. From point of the stability constants of metal with amino groups complexes, the stability constants of Zn^{2+} and Mn^{2+} are the smallest, so they should hardly interfere the detection of lead ions [51]. In aqueous phase, Cu^{2+} and Fe^{3+} may form coordination bonds with amino groups from MHPAM [52], which may influence the fluorescence signals of lead ions sensor. However, the special states of copper and iron ions in the blood environment make them hardly affect the detection of lead ions by sensor. The possible reason is that copper ions exist mainly in the form of ceruloplasmin in the blood. The structure of ceruloplasmin is shown in Fig. S6 A, where copper ions are located in the interior of ceruloplasmin and coordinate completely [53]. In addition, the iron ions are located in the interior of hemoglobin and completely coordinated (Fig. S6B) [54], which is almost difficult to coordinate with the amino group of

MHPAM. Most of the lead ions in the blood are located outside the hemoglobin (Figure S6C) [55], so they can contact the amino group in MHPAM and coordinate with it to form a response signal.

Therefore, it can be inferred that in the whole blood, the presence of the above metal ions (such as Mn^{2+}, Zn^{2+}, Cu^{2+}, Fe^{3+}) has less interference on the detection of lead ions by sensors.

To verify the above hypothesis, we designed the following experiments: Individual ions (Pb^{2+}, Mn^{2+}, Zn^{2+}, Cu^{2+}, Fe^{3+}) and mixed ions (Pb^{2+}+Mn^{2+}, Pb^{2+}+ Zn^{2+}, Pb^{2+}+ Cu^{2+}, Pb^{2+}+ Fe^{3+}) in water and in whole blood were detected by fluorescence biosensor. As shown in Fig. S7A and S7B, the fluorescence sensor has a certain response signal to copper ion and iron ion, but no response signal to manganese and zinc ions in aqueous solution. Fig. S7C and S7D show the change of lead ion signal detected by sensor under mixed aqueous phase ion condition. Among them, manganese and zinc ions have little effect on the detection of lead ion while copper and iron ions will cause slight influence in the detection of lead ion. This result is in good coincide with the above assumptions. Next, the response signals of fluorescence sensor to individual ions in the whole blood (Fig. S7E and S7F). The results show that the fluorescence signal of the sensor cannot be changed by other ions except lead ion. Moreover, the detection results of the sensor under mixed ion conditions in blood environment also show that these metal ions hardly change the response signal (Fig. S7G and S7H). In brief, the above results confirm our hypothesis that the special form of lead ion in the whole blood is an important reason for the selective detection of lead ion by the biosensor.

Based on the above assumptions and experimental results, we also detected the interference of heavy metal ions on the signals of electrochemical sensors in the whole blood environment. As shown in Fig. S8, the mixed heavy metal ions in the blood environment hardly affect the electrochemical signal of the sensor, which further confirms the reasonableness of the above hypothesis.

As show in Fig. S9, through 200 cycles of CV, which showed an almost overlap curves in current intensity indicating good cycle stability of the biosensor. It may be attributed to the strong magnetic force between MHPAM-H and the magnetic electrode, which can make the material firmly fixed on the surface of the electrode, providing a guarantee for the long-term use of the

biosensor.

3.7 Real samples analysis

In order to test the reliability and practical applicability of the dual-responsive biosensor, real blood samples with lead contamination were tested by the biosensor, which is compared with the data obtained by traditional ICP detection. The accuracy and precision of the dual-responsive biosensor are summarized in Table 1. The accuracies of the dual-responsive biosensor are 7.9%, 10.3% for electrochemical detection and 5.9%, 8.9% for fluorescence detection are acceptable, which are less than 15% and can be considered as acceptable data [56]. And RSD values varied from 0.3 to 0.9 for electrochemical detection and from 0.3 to 0.8 for fluorescence detection. The low RSD values indicated that the developed method has a high precision [57, 58].

Table 1. The comparison of blood lead concentration measured by different methods (n=3).

ICP (pM)	**Electrochemical detection**			**Fluorescence detection**		
Expected result (pM)	Obtained result [a] (pM)	Precision[b] (%)	Accuracy[c] (%)	Obtained result[a] (pM)	Precision[b] (%)	Accuracy[c] (%)
6.8	6.1±0.03	0.9	10.3	6.4±0.03	0.8	5.9
54.1	49.8±0.07	0.3	7.9	49.3±0.07	0.3	8.9

[a]Mean ± standart error, [b]Precision %: Relative standard deviation (RSD), [c] Accuracy %: [(Obtained result - Expected result)/ Expected result]×100%.

Moreover, the lead ion standard solution (4.8×10^9 pM, National Nonferrous Metals and Electronic Materials Analysis and Testing Center, Beijing Yihua Tongbiao Technology Co., Ltd.) and diluted it to 4.8×10^3 pM as certified reference materials. As shown in Fig. S10 and Table S3, the average concentration determined by the electrochemical sensor is 5.0×10^3 pM and the average concentration determined by fluorescence sensor is 4.6×10^3 pM after three measurements. The relative error between the values measured by electrochemical, fluorescence sensors and expected result are 4.2% and 8.6%. The above results indicating the potential application of the

dual-responsive biosensor.

4. Conclusions

In summary, we have successfully developed an ultrasensitive, stable, selective and multifunctional biosensor for blood lead detection possessing the ability to rapidly accumulate blood lead within short time and good biofouling resistance ability in blood. Compared with other reported sensors, which are often used in aqueous condition, wide linear relationship and low detection limit can be realized by the dual-biosensor when detecting blood lead. The sensor we designed has wide linear relationship (1.5-4.8×10^3 pM for electrochemical detection and 0.5-4.8×10^3 pM for fluorescent detection) and low detection limit (4.4 pM for electrochemical detection and 1.0 pM for fluorescent detection). It will offer a novel platform for high efficiency detection of whole blood components.

Acknowledgments

Funding: The work was supported by Jiangsu Collaborative Innovation Center of Biomedical Functional Materials, National Natural Science Foundation of China [51641104, 21603105, 21571104]; Research funding of Nanjing Normal University, Jiangsu Key Technology RD Program [BE2016010]; China [BE2015603]; Jiangsu agricultural science and Technology Innovation Fund Project [CX(14)2127]; Technology Support Program of Science and Technology Department of Jiangsu Province [BE2015703]; HuaianBiofunctional Materials and Analysis Technology Innovation Platform [HAP201612].

Competing Interests

The authors have declared that no competing interest exists.

Author contributions

C. M.: Conceptualization; Funding acquisition; Project administration; Writing - review & editing.

M.M.W.: Conceptualization; Writing - original draft; Writing - review & editing.

H. C.: Writing - original draft; Data curation; Formal analysis; Resources; Visualization;

S. B. S., Y.Q.Y, Y. Y. H.: Data curation; Formal analysis; Resources; Visualization;

X. T. Z., S. Y. Z., J. F., Y. J. G.: Software; Data curation; Resources;

B. C.: Methodology.

Appendix A. Supplementary data

Supplementary data associated with this article can be found in the online version.

References

[1] L. Campbell, D.G. Dixon, R.E. Hecky, A review of mercury in Lake Victoria, East Africa: implications for human and ecosystem health, J. Toxicol. Environ. Health. Part B. 6 (2003) 325-356.

[2] W. Jedrychowski, F. Perera, J. Jankowski, V. Rauh, E. Flak, K. L. Caldwell, R. L. Jones, A. Pac, I. Lisowska-Miszczyk, Prenatal low-level lead exposure and developmental delay of infants at age 6 months (Krakow inner city study), Int. J. Hyg. Environ. Health. 211 (2008) 345-351.

[3] C.M.L. Carvalho, E.H. Chew, S.I. Hashemy, J. Lu, A. Holmgren, Inhibition of the human thioredoxin system a molecular mechanism of mercury toxicity, J. Biol. Chem. 283 (2008)

11913-11923.

[4] N.C. Papanikolaou, E.G. Hatzidaki, S. Belivanis, G.N. Tzanakakis, A.M. Tsatsakis, Lead toxicity update. A brief review, Med, Sci. Monitor. 11 (2005) 329-336.

[5] K.L. Caldwell, P.Y. Cheng, J.M. Jarrett, A. Makhmudov, K. Vance, C.D. Ward, R.L. Jones, M.E. Mortensen, Measurement challenges at low blood lead levels, Pediatrics. 2 (2017) 0272-0281.

[6] Z. Wang, D.M. Fang, Q. Li, L.X. Zhang, R. Qian, Y. Zhu, H.Y. Qu, Y.P. Du, Modified mesoporous silica materials for on-line separation and preconcentration of hexavalent chromium using a microcolumn coupled with flame atomic absorption spectrometry, Anal. Chim. Acta 725 (2012) 81-86.

[7] Y. Bakircioglu, S.R. Segade, E.R. Yourd, J.F. Tyson, Evaluation of Pb-Spec (R) for flow-injection solid-phase extraction preconcentration for the determination of trace lead in water and wine by flame atomic absorption spectrometry, Anal. Chim. Acta 485 (2003) 9-18.

[8] M.M. Wan, J. Zhang, Q. Wang, S.Y. Zhan, X.D. Chen, C. Mao, Y.H. Liu, J. Shen, In situ growth of mesoporous silica with drugs on titanium surface and its biomedical applications, ACS Appl. Mater. Interfaces 9 (2017) 18609-18618.

[9] M. Li, D.W. Li, Y.T. Li, D.K. Xu, Y.T. Long, Highly selective in situ metal ion determination by hybrid electrochemical "adsorption-desorption" and colorimetric methods, Anal. Chim. Acta 701 (2011) 157-163.

[10] S. Baghdadi, M. Crozet, S. Gracia, J.L. Dautheribes, C. Riviera, S. Picart, The importance of post-analysis data processing in ICP-AES: calibration adjustment and multi-line approaches, J. Anal. At. Spectrom. 33 (2018) 1903-1909.

[11] H.R. Badiei, C. Liu, V. Karanassios, Taking part of the lab to the sample: On-site electrodeposition of Pb followed by measurement in a lab using electrothermal, near-torch vaporization sample introduction and inductively coupled plasma-atomic emission spectrometry, Microchem. J. 108 (2013) 131-136.

[12] G. Mai, L. Xia, W. X. Wang, Electrochemical detection of blood lead based on the enhancement effect of copper, Russ. J. electrochem. 49 (2013) 447-452.

[13] W.Z. Tang, J.X. Yang, F. Wang, J.L. Wang, Z.H. Li, Thiocholine-triggered reaction in personal glucose meters for portable quantitative detection of organophosphorus pesticide, Anal. Chim. Acta 1060 (2019) 97-102.

[14] Z.G. Liu, Y.F. Sun, W.K. Chen, Y. Kong, Z. Jin, X. Chen, X. Zheng, J.H. Liu, X.J. Huang, S. H. Yu, Facet-dependent stripping behavior of Cu_2O microcrystals toward lead ions: a rational design for the determination of lead ions, Small. 11 (2015) 2493- 2498.

[15] H. Wang, Y. Kim, H. Liu, Z. Zhu, S. Bamrungsap, W. Tan, Combination of a sample pretreatment microfluidic device with a photoluminescent graphene oxide quantum dot sensor for trace lead detection, J. Am. Chem. Soc. 131 (2009) 8221-8226.

[16] X.Y. Xie, Y.Q. Chai, Y.L. Yuan, R. Yuan, Dual triggers induced disassembly of DNA polymer decorated silver nanoparticle for ultrasensitive electrochemical Pb^{2+} detection, Anal. Chim. Acta 1034 (2018) 56-62.

[17] Y. Wen, C. Peng, D. Li, L. Zhuo, S. He, L. Wang, Q. Huang, Q.H. Xu, C. Fan, Metal ion-modulated graphene-DNAzyme interactions: design of a nanoprobe for fluorescent detection of lead(II) ions with high sensitivity, selectivity and tunable dynamic range, Chem. Commun. 47 (2011) 6278-6280.

[18] J. Xia, M. Lin, X. Zuo, S. Su, L. Wang, W. Huang, C. Fan, Q. Huang, Metal ion-mediated assembly of DNA nanostructures for cascade fluorescence resonance energy transfer-based fingerprint analysis, Anal. Chem. 86 (2014) 7084-7087.

[19] T.T. Xu, B. Chi, F. Wu, S.S. Ma, S.Y. Zhan, M.H. Yi, H. Xu, C. Mao, A sensitive label-free immunosensor for detection α-Fetoprotein in whole blood based on anticoagulating magnetic nanoparticles, Biosens. Bioelectron. 95 (2017) 87-93.

[20] L.L. Liang, F.F. Lan, S.G. Ge, J.H. Yu, N. Ren, M. Yan, Metal-enhanced ratiometric fluorescence/naked eye bimodal biosensor for lead ions analysis with bifunctional nanocomposite probes, Anal. Chem. 89 (2017) 3597-3605.

[21] J. Cao, Y.B. Tan, Y.J. Che, H.P. Xin, Novel complex gel beads composed of hydrolyzed polyacrylamide and chitosan: An effective adsorbent for the removal of heavy metal from aqueous solution, Bioresource Technol. 101 (2010) 2558-2561.

[22] W. Yang, C.Y. Pan, M.D. Luo, H.B. Zhang, Fluorescent mannose-functionalized hyperbranched poly(amido amine)s: synthesis and interaction with E. coli, Biomacromolecules 11 (2010) 1840-1846.

[23] F. Ma, W. Li, L. Wang, C.C. Chang, Isolation and identification of the sulphate-reducing bacteria strain H^1 and its function for hydrolysed polyacrylamide degradation, Inte. J. Biotechnol. 10 (2008) 55-56.

[24] C.F. Wu, B. Bull, C. Szymanski, K. Christensen, J. McNeill, Multicolor conjugated polymer dots for biological fluorescence imaging, ACS Nano 2 (2008) 2415-2423.

[25] M.F. Maitz, J. Zitzmann, J. Hanke, C. Renneberg, M.V. Tsurkan, C. Sperling, U. Freudenberg, C. Werner, Adaptive release of heparin from anticoagulant hydrogels triggered by different

blood coagulation factors, Biomaterials 135 (2017) 53-61.

[26] Y.L. Niu, T. Yang, S.S. Ma, F. Peng, M.H. Yi, M.M. Wan, C. Mao, J. Shen, Label-free immunosensor based on hyperbranched polyester for specific detection of α-fetoprotein, Biosens. Bioelectron. 92 (2017) 1-7.

[27] T.T. Xu, B. Chi, M.L. Chu, Q.C. Zhang, S.Y. Zhan, R.J. Shi, H. Xu, C. Mao, Hemocompatible ε-polylysine-heparin microparticles: A platform for detecting triglycerides in whole blood, Biosens. Bioelectron. 99 (2018) 571-577.

[28] H. Zhao, L. Hou, Y.X. Lu, Electromagnetic shielding effectiveness and serviceability of the multilayer structured cuprammonium fabric/polypyrrole/copper (CF/PPy/Cu) composite, Chem. Eng. J. 297 (2016) 170-179.

[29] J.H. Wang, S.R. Zheng, Y. Shao, J.L. Liu, Z.Y. Xu, D.Q. Zhu, Amino-functionalized Fe_3O_4@SiO_2 core-shell magnetic nanomaterial as a novel absorbent for aqueous heavy metals removal, J. Colloid. Interf. Sci. 394 (2010) 293-299.

[30] A. Dalvand, R. Nabizadeh, M.R. Ganjali, M. Khoobi, S. Nazmara, A.H. Mahvi, Modeling of reactive blue 19 azo dye removal from colored textile wastewater using L-arginine functionalized Fe3O4 nanoparticles: optimization, reusability, kinetic and equilibrium studies, J. Magn. Magn. Mater. 404 (2016) 179-189.

[31] L. Montanaroa, C.R. Arciola, E. Cenni, G. Ciapetti, F. Saviolia, F. Filippini, L.A. Barsantic, Cytotoxicity, blood compatibility and antimicrobial activity of two cyanoacrylate glues for surgical use, Biomaterials 22 (2000) 59-66.

[32] M.D. Shastri, G.M. Peterson, R.P. Patel, Redefining approaches to asthma: bridging the gap between heparin and its anti-inflammatory activities, Curr. Allergy. Asthm. R. 17 (2017)

70-86.

[33] X. Kong, Z.L. Qiu, C.E. Lin, Y.Z. Song, B.K. Zhu, L.P. Zhu, X.Z. Wei, High permselectivity hyperbranched polyester/polyamide ultrathin films with nanoscale heterogeneity, J. Mater. Chem. A 5 (2017) 7876-7884.

[34] F.Y. Tong, X.H. Chen, L.B. Chen, P.Y. Zhu, J.F. Luan, C. Mao, J.C. Bao, J. Shen, Preparation, blood compatibility and anticoagulant effect of heparin-loaded polyurethane microspheres, J. Mater. Chem. B 1 (2013) 447-453.

[35] A. Kuzmov, T. Minko, Nanotechnology approaches for inhalation treatment of lung diseases. J. Control. Release. 219 (2015) 500-518.

[36] E. Yeom, J.H. Park, Y.J. Kang, S.J. Lee, Microfluidics for simultaneous quantification of platelet adhesion and blood viscosity, Sci. Rep. 6 (2016) 24994-25000.

[37] Pajkossy, T., Analysis of quasi-reversible cyclic voltammograms: Transformation to scan-rate independent form, Electrochem. Commun. 90 (2018) 69-72.

[38] Y.F. Zhou, Z.X. Wang, Z.Y. Pan, L. Liu, J.Y. Xi, X.L. Luo, Y. Shen, Exceptional performance of hierarchical Ni–Fe (hydr)oxide@NiCu electrocatalysts for water splitting, Adv. Mater. 12 (2018) 1806769-1806777.

[39] R. Elshafey, C. Tlili, A. Abulrob, A.C. Tavares, Label-free impedimetric immimosensor for ultrasensitive detection of cancer marker murine double minute 2 in brain tissue, Biosens. Bioelectron. 39 (2013) 220-225.

[40] T. Bligaard, J.K. Nørskov, Ligand effects in heterogeneous catalysis and electrochemistry, Electrochim. Acta. 52 (2007) 5512-5516.

[41] M. Mostafavi, M.R. Yaftian, F. Piri, H. Shayani-Jam, A new diclofenac molecularly imprinted

electrochemical sensor based upon a polyaniline/reduced graphene oxide nano-composite, Biosens. Bioelectron. 122 (2018) 160-167.

[42] X.F. Sui, X.L. Feng, J. Song, M.A. Hempenius, G.J. Vancso, Electrochemical sensing by surface-immobilized poly(ferrocenylsilane) grafts, J. Mater. Chem. 22 (2012) 11261-11267.

[43] C.F. Wu, C. Szymanski, J. McNeill, Preparation and encapsulation of highly fluorescent conjugated polymer nanoparticles, Langmuir 22 (2006) 2956-2960.

[44] C.H. Wang, C. Yang, Y.Y. Song, W. Gao, X.H. Xia, Adsorption and direct electron transfer from hemoglobin into a three-dimensionally ordered macroporous gold film, Adv. Funct. Mater. 15 (2005) 1267-1275.

[45] T. Yoshitomi, R. Suzuki, T. Mamiya, H. Matsui, A. Hirayama, Y. Nagasaki, pH-sensitive radical-containing-nanoparticle (rnp) for the l-band-epr imaging of low ph circumstances, Bioconjugate Chem. 209 (2009) 1792-1798.

[46] Z.L. Li, Y.Y. Ge, L. Wan, Fabrication of a green porous lignin-based sphere for the removal of lead ions from aqueous media, J. Hazard. Mater. 285 (2015) 77-83.

[47] M.M.Wan, T.T. Xu, B. Chi, M. Wang, Y.Y. Huang, Q. Wang, T. Li, W.Q. Yan, H. Chen, P. Xu, C. Mao, B. Zhao, J. Shen, H. Xu, D.Q. Shi, A safe and efficient strategy for the rapid elimination of blood lead in vivo based on a capture-fix-separate mechanism, Angew. Chem. Int. Ed. 58 (2019) 10582-10586.

[48] J.L. Liu, L.L. Lu, A.Q. Li, J. Tang, S.G. Wang, S.Y. Xu, L.Y. Wang, Simultaneous detection of hydrogen peroxide and glucose in human serum with upconversion luminescence, Biosens. Bioelectron. 68 (2015) 204-209.

[49] J.C. Xu, J.P. Xiao, M. Jiang, C.Q. Qin, L.T. Zeng, H. Zhang, J.F. Zhang, A

mitochondria-targeted ratiometric fluorescent probe for rapid, sensitive and specific detection of biological SO_2 derivatives in living cells, Biosens. Bioelectron. 77 (2016) 725-732.

[50] J. Ju, W. Chen, In situ growth of surfactant-free gold nanoparticles on nitrogen-doped graphene quantum dots for electrochemical detection of hydrogen peroxide in biological environments, Anal. Chem. 873 (2015) 1903-1910.

[51] H. Irving, R.J.P. Williams, Order of Stability of Metal Complexes, Nature 162 (1948) 746-747.

[52]S. Conradi, C. Vogt, H. Wittrisch, G. Knobloch, G. Werner, Capillary electrophoretic separation of metal ions using complex forming equilibria of different stabilities, J. Chromatogr. A 754 (1996) 103-109.

[53] P. Vachette, E. Dainese, V.B. Vasyliev, P.D. Muro, M. Beltramini, D.I. Svergun, V.D. Filippis, B. Salvato, A key structural role for active site type 3 copper ions in human ceruloplasmin, J. Biol. Chem. 277 (2002) 40823-40831.

[54] K. Varmira, O. Abdi, M.-B. Gholivand, H.C. Goicoechea, R. Jalalvand, Intellectual modifying a bare glassy carbon electrode to fabricate a novel and ultrasensitive electrochemical biosensor: Application to determination of acrylamide in food samples, Talanta 176 (2018) 509-517.

[55] N. C. N. Chan, K. P. Chan, Coarse basophilic stippling in lead poisoning, Blood 129 (2017) 3270.

[56] R.A. Sutherl, F.M.G.Tack, Determination of Al, Cu, Fe, Mn, Pb and Zn in certified reference materials using the optimized BCR sequential extraction procedure, Anal. Chim. Acta, 454 (2002) 249-257.

[57] M.L. Yola, T. Eren, N. Atar, A sensitive molecular imprinted electrochemical sensor based on gold nanoparticles decorated graphene oxide: Application to selective determination of tyrosine in milk, Sensor. Actuat. B-Chem. 210 (2015) 149-157.

[58] M.M. Wan, Y.Y. Li, T. Yang, T. Zhang, X.D. Sun, J.H. Zhu, In situ loading of drugs into mesoporous silica SBA-15, Chem. Eur. J. 22 (2016) 6294-6301.

Graphical Abstract

A dual-responsive biosensor for blood lead detection

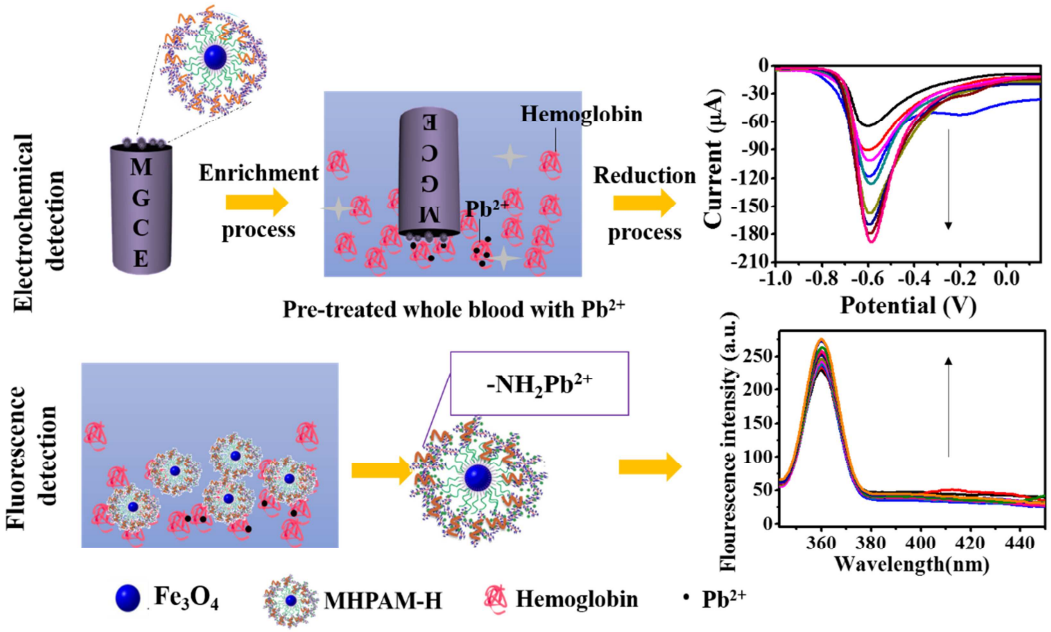

Declaration of interests

☒ The authors declare that they have no known competing financial interests or personal relationships that could have appeared to influence the work reported in this paper.

☐The authors declare the following financial interests/personal relationships which may be considered as potential competing interests:

Research highlights:

- A novel dual-responsive electrochemical/fluorescent biosensor.
- Hyperbranched polyamide with heparin modification (MHPAM-H) for blood lead detection.
- The method displays a good linear relationship (1.5-4.8×10^3 pM for electrochemical detection and 0.5 pM-4.8×10^3 pM for fluorescent detection) with low detection limit (4.4 pM for electrochemical detection and 1.0 pM for fluorescent detection) for blood lead and acceptable accuracy, precision.